Research Square

Preprints are preliminary reports that have not undergone peer review.
They should not be considered conclusive, used to inform clinical practice,
or referenced by the media as validated information.

Explaining the “Missing Loss” Process in Earth’s Magnetosphere

Bernhard Haas

bhaas@gfz.de

GFZ Helmholtz Centre for Geosciences

Yuri Y. Shprits

GFZ Helmholtz Centre for Geosciences

Alexander Y. Drozdov

The Aerospace Corporation

Dedong Wang

GFZ Helmholtz Centre for Geosciences

Alwin Roy

GFZ Helmholtz Centre for Geosciences

Katja Stoll

GFZ Helmholtz Centre for Geosciences

Xingzhi Lyu

GFZ Helmholtz Centre for Geosciences

Article

Keywords:

Posted Date: November 2nd, 2026

DOI: https://doi.org/10.21203/rs.3.rs-11240727/v1

License: This work is licensed under a Creative Commons Attribution 4.0 International License.
Read Full License

Additional Declarations: No competing interests reported.

Explaining the "Missing Loss" Process in Earth's Magnetosphere

Bernhard Haas*[1,2], Yuri Y. Shprits[1,2], Alexander Y. Drozdov[4], Dedong Wang[1], Alwin Roy[1,2], Katja Stoll[1,2,5], and Xingzhi Lyu[1]

[1]GFZ Helmholtz Centre for Geosciences, Potsdam, Germany
[2]Institute for Physics and Astronomy, University of Potsdam, Potsdam, Germany
[4]The Aerospace Corporation, El Segundo, CA, USA
[5]German Aerospace Center (DLR), Institute for Solar-Terrestrial Physics, Neustrelitz, Germany

September 1, 2026

Abstract

The dynamics of the Earth's electron ring current are governed by a complex balance between transport, acceleration, and loss. Despite decades of modeling, a persistent discrepancy remains: physics-based simulations consistently overestimate electron fluxes by up to two orders of magnitude. The current theories fail to explain this "missing loss" process. Here, we demonstrate that no additional loss process is required to explain this apparent mismatch between theory and observations; rather, the discrepancy arises from neglecting the variability of the background plasma density. By coupling a time-dependent plasma density model with a ring current simulation, we show that density depletions modulate the plasma wave dispersion relation, enhancing electron precipitation by a factor of 100. This increase in loss rates explains the difference between theoretical predictions and satellite observations. Our results reveal that background plasma density, rather than wave intensity alone, is a primary driver of magnetospheric particle loss, providing a vivid example of how cold plasma density can influence the loss of particles that are up to 10,000 times more energetic than the cold plasma itself.

The ring current, a toroidal region composed of energetic charged particles encircling the Earth, plays a crucial role in magnetospheric dynamics and has a pronounced effect on the ground. Ring current enhancements lead to a significant decrease of the geomagnetic field[1,2]. While the existence of the ring current was already hypothesized in the early 20th century[3,4], it was first observed in situ in 1966 by the OGO-3 satellite[5]. It is now understood that the ring current is primarily composed of ions and electrons with energies ranging from a few keV to hundreds of keV. High solar activity increases the electric field associated with the solar wind. This electric field maps into the magnetosphere and energizes particles, which contribute to the ring current, causing its intensity to increase by several orders of magnitude[6]. During these times, also called geomagnetic storms, electrons are most hazardous to the electrical components and solar panels of satellites due to surface charging effects[7]. The enhancement of the ring current is counteracted by scattering of electrons into the atmosphere due to interactions with whistler-mode plasma waves[8], altering the atmosphere's chemistry and contributing to ozone depletion in the polar regions[9].

Significant modeling efforts have been dedicated to understanding the transport, acceleration, and loss mechanisms governing the electron ring current[10]. While the source of ring current electrons in the inner magnetosphere is relatively well understood, the current models do not fully reproduce the observed loss of electrons[11,12]. More specifically, a persistent discrepancy remains: physics-based simulations consistently overestimate electron fluxes by over two orders of magnitude compared to in-situ satellite observations during strong geomagnetic storms[13,14]. It was theorized that a "missing loss" process, not accounted for in current models, could be responsible for this discrepancy[14]. This lack of scattering has also been confirmed by Low-Earth-Orbit observations[12], but these observations have also failed to reveal the physical mechanism

*Corresponding author: bhaas@gfz.de

responsible for this loss process. More recently, other types of waves, such as electron cyclotron harmonics and time domain structures, have been tested as potential candidates for the missing loss process, but their contribution has been found to be insufficient to explain the observed loss of particles[15,16].

Here, we demonstrate that the "missing loss" is not a missing wave mode, but results from the neglect of the coupling between the cold plasma background and the energetic ring current electrons (see Fig. 1). We present global simulations of the Earth's ring current during the March 2013 geomagnetic storm, coupling a time-dependent plasma density model with a ring current simulation. We show that density depletions significantly affect the plasma wave dispersion relation, shifting the resonance condition and allowing waves to interact with higher-energy particles. This shift in resonance increases electron precipitation by up to two orders of magnitude. This enhanced scattering effectively resolves the apparent overestimation of electron fluxes.

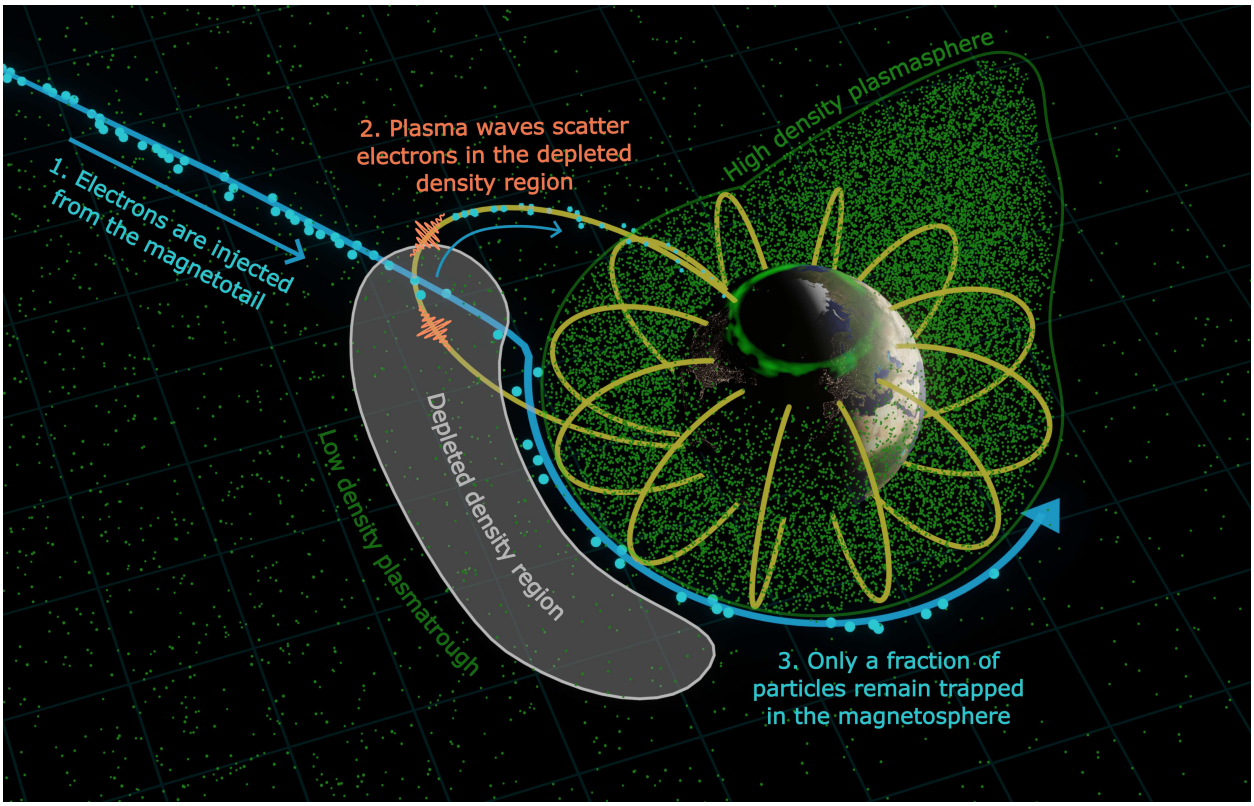


Figure 1: Schematic of electron loss proposed in this study.

Increased Scattering under low background density conditions

Particles in the Earth's magnetosphere are trapped by the geomagnetic field and organized by their equatorial pitch angle: the angle between the particle momentum and the background magnetic field as it crosses the magnetic equator. Particles with 90° equatorial pitch angle are trapped at the magnetic equator, while particles with smaller equatorial pitch angles are mirroring between the northern and southern hemispheres. By interacting with plasma waves, the mirror point of particles can be lowered to the atmosphere, where they will collide with atmospheric particles and will be lost from the system. This process leads to the evolution of the electron phase space density f governed by the pitch-angle diffusion equation:

$$\frac{\partial f}{\partial t} = \frac{1}{\sin(2\alpha)T(\alpha)} \frac{\partial}{\partial \alpha} \left(\sin(2\alpha) T(\alpha)\, D_{\alpha\alpha} \frac{\partial f}{\partial \alpha} \right) - \frac{f}{\tau_{LC}}, \tag{1}$$

where α is the equatorial pitch angle, $T(\alpha) = 1.38 - 0.32(\sin\alpha + \sin^{1/2}\alpha)$ is a function related to the particles' bounce frequency[17], $D_{\alpha\alpha}$ is the bounce-averaged diffusion coefficient due to scattering by whistler-

mode plasma waves, and τ_{LC} is the quarter-bounce period, which is the average time field-aligned particles will spend before being lost to the atmosphere. The trigonometric functions arise from the averaging of the diffusion equation over the particles' bounce period.

To quantify the sensitivity of our results to the assumed plasma density, we performed two sets of simulations with constant and variable background plasma density. In these simulations, we calculate bounce-averaged diffusion coefficients ($D_{\alpha\alpha}$ in Eq. 2) for two distinct scenarios: a baseline representing long-term average density and a "depleted" case corresponding to observations during intense geomagnetic activity [18,19]. For the depleted case, we assume that the density is 4 times lower than the average values consistent with observations [20]. As shown in Fig. 2A, for the low-density regime at low pitch angles, the diffusion coefficients reflecting depleted density values are up to two orders of magnitude higher than the diffusion coefficients for average density values. Since the rate of electron precipitation is primarily governed by scattering at small pitch angles [21], as it can create a bottleneck in scattering, this increase in pitch-angle scattering results in a dramatic increase in loss. Rapid loss depletes the ring current electrons at timescales comparable to an hour (Fig. 2C).

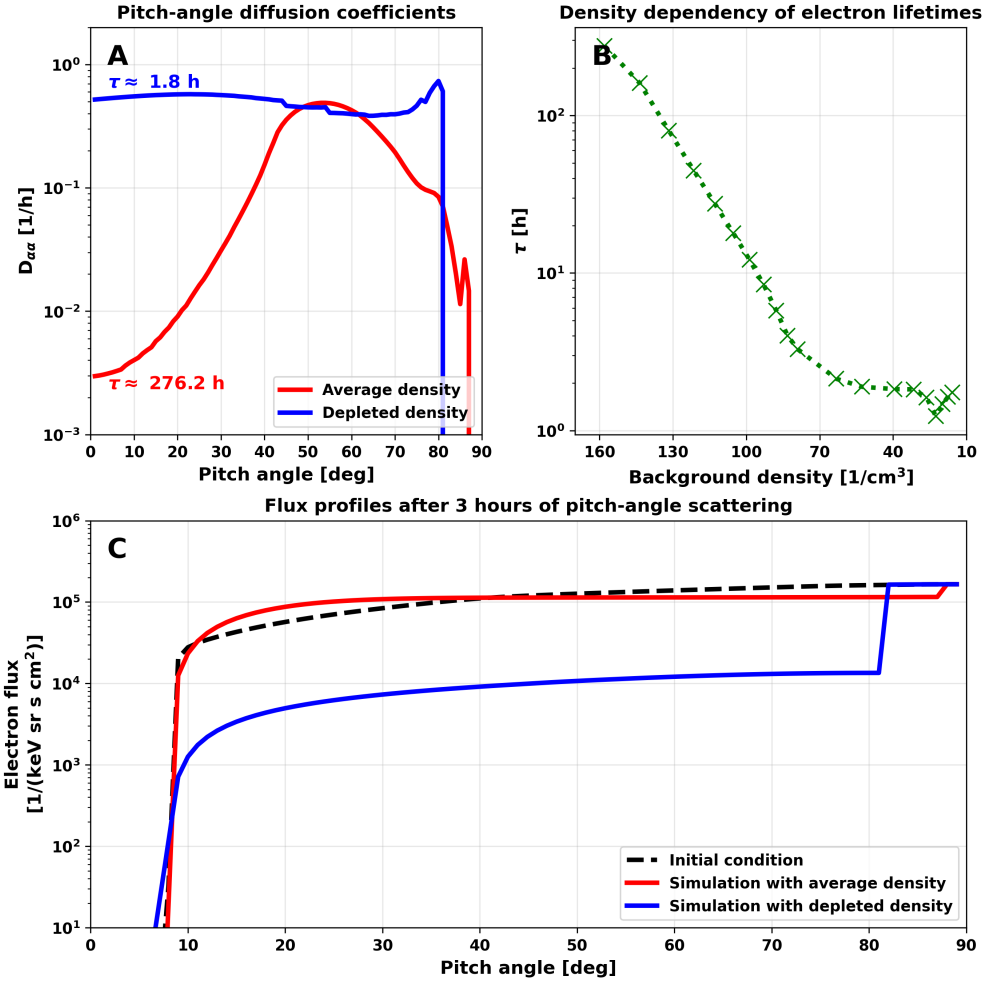


Figure 2: Diffusion coefficients and flux as a function of pitch angle at the end of the 3-hour simulation for average and depleted density conditions (lower by a factor of 4). The diffusion rates are calculated for 9 keV, L of 3, and magnetic local time of 21 hours. **A** Pitch-angle diffusion coefficients by chorus waves. **B** Density dependency of the scattering rates into Earth's atmosphere. **C** Flux evolution predicted by the diffusion coefficients.

Changes in the background density n_e alter the plasma wave dispersion relation, $k^2(\omega) \propto \omega_{pe}^2$, through

scaling of the plasma frequency $\omega_{pe} \propto \sqrt{n_e}$. Assuming parallel propagation for whistler-mode chorus waves and considering the first-order cyclotron resonance in the non-relativistic case, the resonance condition is defined as $v_\parallel = (\omega - \Omega_e)/k$, where $v_\parallel$ is the parallel velocity of the resonant particle and $\Omega_e = eB/m_e$ is the electron cyclotron frequency. A reduced density results in a smaller wave number k for a given frequency ω, causing a shift in the resonance condition towards particles with higher $v_\parallel$. This mechanism effectively increases the scattering rates of particles with higher energies and lower pitch angles, scattering more field-aligned electrons into the atmosphere. The shift in the resonance is visible in the diffusion coefficients plotted for varying density levels (see Supplementary Fig. S1 and S2).

The dependency of wave-particle interactions on the background plasma density has been known since the formulation of the quasi-linear theory[22,23]. However, due to the complexity of calculating the scattering rates and the multitude of input parameters, such as the distributions of waves in frequency and wave-normal angle, the diversity of the wave spectrum, and the spatial distribution of waves, the density dependence has been largely ignored. The shift in resonances illustrated above for a high plasma density and field-aligned waves, is not very obvious in realistic cases.

In more recent years, studies discussed how diffusion coefficients depend on the background plasma density[20,24], and that wave-particle interactions in low-density regions are responsible for accelerating electrons to ultra-relativistic energies in the radiation belts[25,26]. These studies focused on relativistic electrons above MeV energies, whereas the effects on ring current particles have not been previously explored. Here, we demonstrate the substantial effect of low-density interactions on particles with energies below 50 keV driven by upper-band chorus waves. As shown in Fig. 2B, in some cases, even a moderate decrease in density by less than a factor of two can increase the scattering rates by an order of magnitude.

Ring current simulations including the plasma density variability for the March 2013 geomagnetic storm

We then investigated whether this localized mechanism could resolve the "missing loss" issue by performing 4D ring current simulations coupled with a plasmasphere model of the March 2013 storm. This storm event was the subject of previous studies highlighting the overestimation of electron fluxes by ring current models[13,14]. The ring current simulation is based on a modified 4D Fokker-Planck equation accounting for radial and azimuthal transport, and local diffusion of phase space density (f)

$$\begin{aligned}\frac{\partial f}{\partial t} =& -\frac{\partial (v_R f)}{\partial R} - \frac{\partial (v_\varphi f)}{\partial \varphi} + \\ &+ \frac{1}{G}\frac{\partial}{\partial V}\bigg|_{K,R} G\left(D_{VV}\frac{\partial f}{\partial V}\bigg|_{K,R} + D_{VK}\frac{\partial f}{\partial K}\bigg|_{V,R}\right) + \\ &+ \frac{1}{G}\frac{\partial}{\partial K}\bigg|_{V,R} G\left(D_{KK}\frac{\partial f}{\partial K}\bigg|_{V,R} + D_{KV}\frac{\partial f}{\partial V}\bigg|_{K,R}\right) - \frac{f}{\tau_{LC}}. \end{aligned} \quad (2)$$

Here, R is the radial coordinate, φ is the magnetic local time, while V and K are modified first and second adiabatic invariants, respectively[27]. The drift velocities in magnetic local time (v_φ) and radial distance (v_R) are calculated from empirical models describing the electric[28–30] and magnetic field[31] in the equatorial plane. The diffusion coefficients D_{VV}, D_{VK}, and D_{KK} represent the scattering and acceleration driven by wave-particle interactions, which we modulate here using time-dependent plasma density. More information about the $V - K$ coordinate system and the Jacobian G is provided in Methods.

The diffusion coefficients vary in space and time based on the current level of geomagnetic activity and, most importantly, the background plasma density.The background plasma density is modeled using a physics-based approach that includes convection and refilling from the ionosphere (see Methods). An example of the large depletion predicted by the plasmasphere model is depicted in Fig. 3, where the plasma density decreases by up to a factor of 7 compared to the statistical model[32]. Crucially, the maximum density depletion predicted by our model coincides spatially with the pre-midnight sector, where stronger electron loss is required to match particle flux observations[14]. The predicted location of the density depletion is consistent with statistical studies of cold plasma density[18].

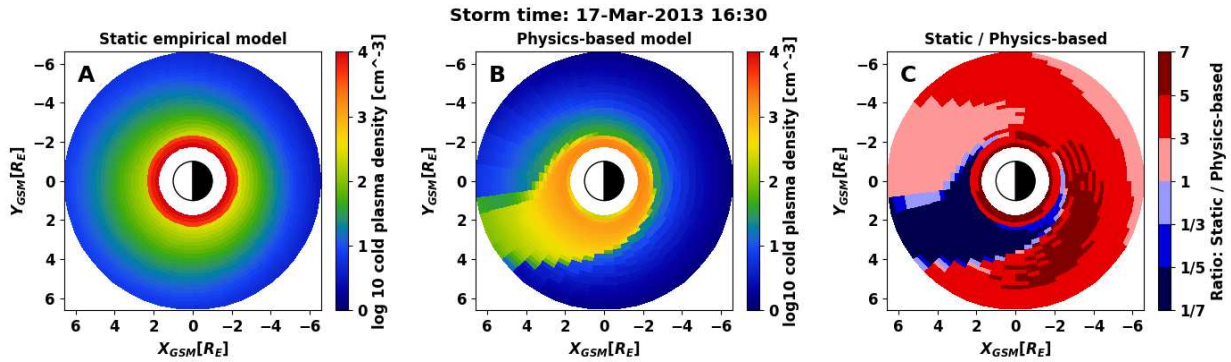


Figure 3: Background density in the equatorial plane during the storm main phase. **A** Density predicted by the static empirical model. **B** Density predicted by the physics-based model. **C** Ratio between the models shown in Panel A and Panel B.

The results of the coupled ring current-plasmasphere simulation are presented in Fig. 4, showing a comparison between simulated and observed electron fluxes in the inner magnetosphere from the RBSP-B satellite. The overestimation of electron fluxes by up to two orders of magnitude is clearly visible in the standard simulation with static background density (Panels C and E). In contrast, the coupled simulation (Panels D and F) shows a significant reduction in electron fluxes at lower radial distances, bringing them into closer agreement with observations. The increased scattering in the pre-midnight sector effectively eliminates the overestimation, demonstrating that the inclusion of background plasma density variability resolves the long-standing discrepancy in ring current models. Validation of the precipitating particles also shows that the inclusion of variable background density improves the comparison to observations taken at low-earth-orbit in the pre-midnight sector (see Supplementary Fig. S3)

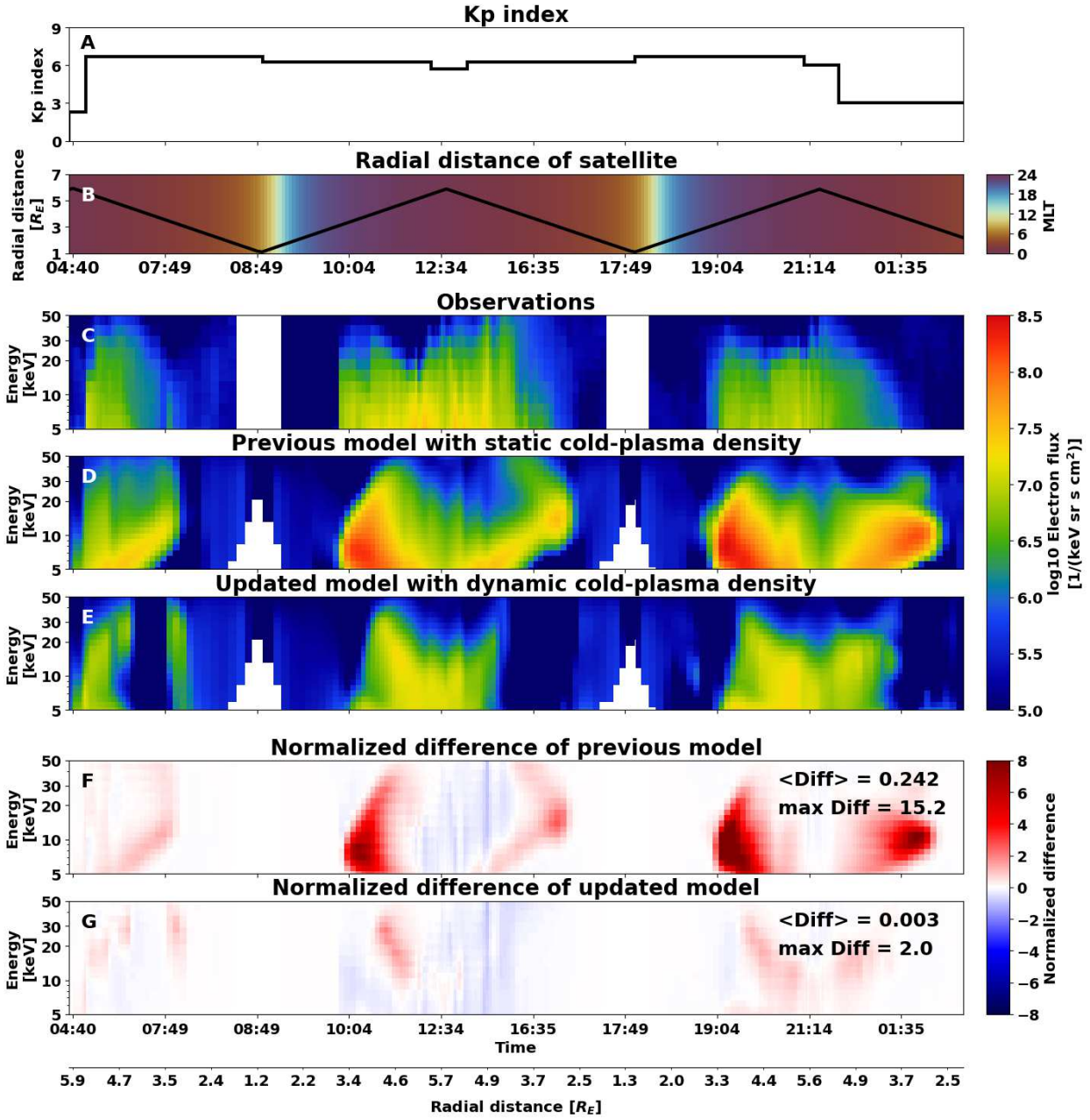


Figure 4: Observations and simulation results of ring current electrons during the March 2013 geomagnetic storm. Data is shown on a modified x-axis which removes the visual bias towards large radial distances[33]. **A** Kp index derived from ground observations and showing the level of geomagnetic activity throughout the storm. **B** Radial distance and magnetic local time of the RBSP-B satellite normalized to Earth radii. **C** RBSP-B HOPE observations of electron flux at 50° local pitch angle and 5 to 50 keV. **D** Simulated electron flux along the satellite orbit by the model with static background density. **E** Simulated electron flux along the satellite orbit by the model with dynamic density predicted by a physics-based model. **F** Normalized difference between C and D. **G** Normalized difference between C and E.

While previous theories focused almost exclusively on wave power as the driver of precipitation, our results demonstrate that even moderate wave intensities, as usually observed in the pre-midnight sector[34], can drive strong loss rates when the background density is lower than the average values that are often assumed for simulations. This suggests that the "missing loss" was not due to an unaccounted-for wave

mode, but missing cross-scale coupling between the cold and hot plasma populations.

These findings have profound implications for space sciences, space weather forecasting, atmospheric chemistry, and climate science. Our results deepen our understanding of energetic electron precipitation, a critical uncertainty in global magnetospheric and atmospheric modeling. By providing a physically consistent mechanism for these loss rates, this work enables more accurate quantification of NOx and HOx production in the upper atmosphere, which are key catalysts for ozone depletion in the polar regions. As highlighted in the IPCC AR6 Working Group I report[35], long-term simulations of electron precipitation are essential for understanding solar-terrestrial coupling and its role in regional climate variability. Moreover, understanding particle loss will allow researchers to quantify the effects of precipitation on ionospheric conductivity, which is central to magnetospheric-ionospheric coupling[36–38]. This provides an important feedback between the cold plasma density, the global magnetosphere, and the ionosphere. Similar processes and density control may be important for the outer planetary and exoplanetary radiation environments, as well as for other astrophysical phenomena related to particle acceleration and loss due to wave-particle interactions.

Methods

Calculation of bounce-averaged diffusion coefficients

The bounce-averaged diffusion coefficients, describing the interactions between chorus waves and electrons, are calculated using the Full-Diffusion-Code (FDC)[39]. Necessary frequency and wave-normal-angle distribution for lower and upper band chorus waves are based on statistical properties derived from satellite observations[34]. We calculated diffusion coefficients for different background density values: the "standard" case of an empirical, static density model[32] as used in previous studies[14,40], and for cases of density depletion, where we assume a global density given by the static density model divided by a constant factor (2 to 10). Thus, we have defined the diffusion coefficients for each energy, equatorial pitch angle, radial distance, magnetic local time, and various density levels, and can use combinations of those matrices to accurately define the diffusion coefficients globally.

Physics-based predictions of the background plasma density

We utilize the VERB-CS (Versatile near-Earth environment of Radiation Belts and ring current - Convection Simplified) model[41] to simulate the time-dependent cold plasma density in the inner magnetosphere. The model incorporates particle transport driven by the large-scale convection electric field, as well as refilling processes from the ionosphere. The following equation is solved for every 15-minute time step to compute the evolution of the cold plasma density n_e:

$$\frac{\partial n_e}{\partial t} = -v_R \frac{\partial n_e}{\partial R} - v_\varphi \frac{\partial n_e}{\partial \varphi} + S - L, \tag{3}$$

where R is the radial coordinate, φ is the magnetic local time, v_R and v_φ are the radial and azimuthal convection velocities derived from the large-scale Volland-Stern electric field[28–30] and T89 magnetic field[31] model, S is an empirical source term representing ionospheric refilling[42], and L are losses to the dayside magnetopause[43]. The spatial grid spans radial distances from 1 to 10 with a resolution of 0.2 Earth radii, and magnetic local time from 0 to 24 hours with a resolution of 0.5 hours. The boundary condition at $R = 10$ is set using an empirical model driven by solar wind parameters[44].

The comparison between the predicted cold plasma density and that measured by the Van Allen Probes is shown in Supplementary Fig. S4. The cold-plasma density is inferred from the magnetic field spectrogram by detecting the upper hybrid frequency, from which the background density can be calculated[45]. The spectrogram during the main phase of the storm is occasionally obscured by electron cyclotron and other broadband emissions, which makes it very challenging to identify the upper hybrid frequency, as stated in the data description[45]. The data should therefore be treated with great care, as large uncertainties are expected for this type of spectrogram.

Coupled ring current-plasmasphere simulations

The density values obtained from the VERB-CS model are integrated into the ring current simulation by updating the bounce-averaged diffusion coefficients at each 15-minute time step. We took the ratio between the predicted density from VERB-CS and the empirical density model[32], and discretized them into 10 levels from 1 to 10. For each level of density depletion, we pre-computed diffusion coefficients as described in the previous section. For each point in space and time outside the plasmapause, the diffusion coefficients are used according to the current density level predicted by VERB-CS and scaled by the current Kp value.

We follow previous studies of the ring current[11,46–49] and assume that energy diffusion is negligible. Thus, D_{pp} and D_{pa} are set to zero before the diffusion coefficients are transformed into the (V, K) coordinate system used by VERB-4D[27]. The potential contribution of energy diffusion at keV energies will be the subject of future studies. V and K are modified adiabatic invariants, built from the first (μ) and second (J) adiabatic invariants[50]:

$$K = \frac{J}{\sqrt{8 m_0 \mu}}, \qquad V = \mu \cdot (K + 0.5)^2, \tag{4}$$

with m_0 being the rest mass of the particles.

These time-dependent diffusion coefficients are then applied to the VERB-4D (Versatile near-Earth environment of Radiation Belts and ring current in four dimensions) model[51], which solves Equation 2 using a 15-minute time step. The VERB-4D model solves the Fokker-Planck equation on a grid of modified adiabatic invariants (V, K), as this system allows for the efficient solving of convection and diffusion on a single numerical grid[27]. For the derivation of the Jacobian G from the adiabatic invariant space to V-K space, we refer to previous publications[52]. The model grid spans radial distances from 1 to 6.6 with a resolution of 0.2 Earth radii, magnetic local time from 0 to 24 hours with a resolution of 0.5 hours, logarithmically-spaced 60 points in energy from 0.1 eV to 100 keV at $R = 6.6$, and 61 points in equatorial pitch angle from 0.7 to 89.7 degrees at $R = 6.6$. The operators of Equation 2 are split into a 2-D convection and a 2-D diffusion step, which are solved sequentially. The convection solver utilizes a 9th-order finite difference scheme in space and a first-order explicit scheme in time[53,54]. The diffusion solver employs an implicit positive-preserving finite volume scheme, ensuring numerical stability and physical consistency[55]. Previous studies have used an implicit finite difference scheme to solve the diffusion equation, including mixed terms; however, this approach failed at some time steps due to negative phase-space density values, leading to numerical instabilities[56,57]. To achieve a realistic distribution within the loss cone, we found it necessary to perform the diffusion step at a sub-time step of 6 seconds due to the fast particle dynamics there.

The initial condition is set using RBSP-B observations prior to the storm onset on March 17, 2013, in agreement with previous studies[14]. The radial boundary condition at geosynchronous orbit is set using an empirical model driven by the Kp index[58], while we set $f = 0$ at $R = 1$. We further apply zero-derivative boundary conditions at the lower and upper boundaries in V, corresponding to no flow over these boundaries. Since we are not modeling local acceleration in this study, the choice of boundary conditions in V has a negligible effect on the results. The upper-K boundary at pitch-angles close to zero is assumed to be a zero-derivative boundary, to allow the modeling of the strong diffusion scenario[59]. A zero-derivative boundary is also applied at the lower-K boundary, which is close to 90° pitch angle to reflect the symmetry of the pitch-angle distribution.

Removing bump-on-tail instabilities from simulation output

As the wave-particle interactions are not treated self-consistently in the VERB-4D model, it is possible that beams form in the velocity distribution of particles, also known as bump-on-tails. These bumps are highly unstable as they lead to the growth of Langmuir waves. As a result, the particles donate their kinetic energy to the wave field, effectively damping the distribution and smoothing the bump until stability is restored.

To capture this relaxation process, we implement an algorithm to detect and remove these features from the phase-space density model output distribution for varying μ and constant K. A bump is identified when the distribution exhibits a sustained positive gradient across at least five consecutive grid points, immediately followed by a negative gradient. A representative example of a corrected distribution is provided in Supplementary Fig. S5. The bump-on-tail instabilities already exist in the simulation assuming static cold-plasma density, but got greatly enhanced when variable density is introduced. For comparison, a version

of Fig. 4 retaining these instabilities is shown in Supplementary Fig. S6. On average, bump removal has little influence on the simulation results, as indicated by the average normalized difference. However, it removes one unphysical feature in the energy spectrogram during the satellite's inbound pass at around 16 UTC. Applying energy diffusion might mitigate these unstable peaks through diffusive smoothing. We suggest that the formation of unstable distributions due to the interplay between wave-particle interactions and particle convection in the magnetosphere should be further investigated in future modeling studies.

The normalized-difference metric

We apply the "normalized difference" metric[60] for the data-model comparison in Fig. 4, as this metric allows us to verify the peak values of the ring current, while less attention is spent on lower flux values. This metric is most suitable for this study, as we are most interested in the peak values, which were previously reported as overestimated[13,14]. The normalized difference N_{diff} is defined as:

$$N_{\text{diff}} = \frac{j_{\text{simulated}} - j_{\text{observed}}}{j_{\text{max observed}}}, \tag{5}$$

where $j_{\text{simulated}}$ is the electron flux predicted by VERB-4D, j_{observed} is the observed flux, and $j_{\text{max observed}}$ is the maximum flux value observed during the simulation period for each energy.

Validation of precipitating flux

For validating the precipitating flux, we followed the processing steps from previous work[12]. The Polar Operational Environmental Satellite (POES) Total Energy Detector (TED) measurements are mapped to the equatorial plane using the T89 magnetic field model[31], and data points below the background level are removed. We sampled the simulations along virtual spacecraft paths using the maximum observed pitch angle, accounting for a field of view of 15°. Predicted fluxes below the instrument noise level were removed in the same manner as the observations. The resulting data were then binned onto a spatial grid with a resolution of 2 hours in MLT and 2/3 R_E in radial distance using the log-averaging. Supplementary Fig. S3 shows a bias (around a factor of 2) between observed and modeled precipitating fluxes using the model with dynamic cold-plasma density. This discrepancy may arise from either a systematic underestimation of electron loss in the model or intercalibration uncertainties in the measurements. Since the VERB-4D model output scales linearly with the LANL-based boundary conditions at GEO[58], the bias could be resolved by a corresponding scaling of the boundary input. We conclude that further intercalibration with the POES TED instrument is required to clarify the source of this discrepancy.

Code Availability

The code used in this study is available at `https://git.gfz-potsdam.de/spsw/verb/verb4d/verb4d_solver` and `https://git.gfz-potsdam.de/spsw/verb/verb4d/verb4dpy`.

Data Availability

The authors acknowledge the NASA OMNI database (https://omniweb.gsfc.nasa.gov/form/dx1.html) and thank the developers of the IRBEM library (https://github.com/PRBEM/IRBEM), which was used for magnetic field calculations. The authors are grateful to the RBSP-ECT team for the provision of Van Allen Probes observations, which are available under `https://spdf.gsfc.nasa.gov/pub/data/rbsp/rbspa/l3/ect/hope/pitchangle/rel04/`. The data processing code is available at `https://github.com/GFZ/EL_PASO`.

Funding Statement

This research has been partially funded by the Deutsche Forschungsgemeinschaft (DFG) - Project-ID 318763901 - SFB1294. This work was supported by the European Research Council (ERC) under the European Union's

Horizon 2020 research and innovative programme (grant agreement number: 101124679-WIRE) and the Deutsche Forschungsgemeinschaft (DFG) through the project "RADIANCE" project no. 547667751. Dedong Wang and Alwin Roy acknowledges the funding support from the Deutsche Forschungsgemeinschaft (DFG) through the project "Understanding the Properties of Chorus Waves in the Earth's Inner Magnetosphere and Their Effects on Van Allen Radiation Belt Electrons" (Chorus Waves) - WA 4323/5-1.

Author Contributions

B.H., Y.S., A.D., D.W., and K.S. had the initial idea for this study and designed the methodology. A.R. calculated density dependent-diffusion coefficients. All authors analyzed the simulation results. B.H. and X.L. wrote the initial draft of the manuscript. All authors reviewed the manuscript.

Competing interests

The authors declare no competing interests.

References

[1] Alexander von Humboldt. Die vollständigste aller bisherigen Beobachtungen über den Einfluss des Nordlichts auf die Magnetnadel. *Annalen der Physik*, 29:425–429, 1808.

[2] David P. Stern. A Millennium of Geomagnetism. *Reviews of Geophysics*, 40(3):1–1–1–30, 2002. ISSN 1944-9208. doi: 10.1029/2000RG000097. URL https://onlinelibrary.wiley.com/doi/abs/10.1029/2000RG000097.

[3] C. Störmer. Sur les trajectoires des corpuscules électrisés dans l'espace sous l'action du magnétisme terrestre, avec application aux aurores boréales. *Le Radium*, 9(11):395–399, November 1912. ISSN 0370-3223. doi: 10.1051/radium:01912009011039501. URL http://dx.doi.org/10.1051/radium:01912009011039501. Publisher: MASSON ET CIE, Editeurs.

[4] S. Chapman and V. C. A. Ferraro. A new theory of magnetic storms. *Terrestrial Magnetism and Atmospheric Electricity*, 38(2):79–96, 1933. ISSN 0096-8013. doi: 10.1029/TE038i002p00079. URL https://onlinelibrary.wiley.com/doi/abs/10.1029/TE038i002p00079.

[5] L. A. Frank. EXTRATERRESTRIAL RING CURRENT DURING GEOMAGNETIC STORMS. *J. Geophys. Res., 72: 3753-67(Aug. 1, 1967).*, January 1967. doi: 10.1029/JZ072i015p03753. URL https://www.osti.gov/biblio/4293304. Institution: Univ. of Iowa, Iowa City.

[6] H. Zhao, X. Li, D. N. Baker, S. G. Claudepierre, J. F. Fennell, J. B. Blake, B. A. Larsen, R. M. Skoug, H. O. Funsten, R. H. W. Friedel, G. D. Reeves, H. E. Spence, D. G. Mitchell, and L. J. Lanzerotti. Ring current electron dynamics during geomagnetic storms based on the Van Allen Probes measurements. *Journal of Geophysical Research: Space Physics*, 121(4):3333–3346, 2016. ISSN 2169-9402. doi: 10.1002/2016JA022358. URL https://onlinelibrary.wiley.com/doi/abs/10.1002/2016JA022358.

[7] Yihua Zheng, Insoo Jun, Weichao Tu, Yuri Y. Shprits, Wousik Kim, Daniel Matthiä, Matthias M. Meier, W. Kent Tobiska, Yoshizumi Miyoshi, Vania K. Jordanova, Natalia Y. Ganushkina, Valeriy Tenishev, T. P. O'Brien, Antoine Brunet, Vincent Maget, Jingnan Guo, Dedong Wang, Richard B. Horne, Sarah Glauert, Bernhard Haas, and Alexander Y. Drozdov. Overview, progress and next steps for our understanding of the near-earth space radiation and plasma environment: Science and applications. *Advances in Space Research*, May 2024. ISSN 0273-1177. doi: 10.1016/j.asr.2024.05.017. URL https://www.sciencedirect.com/science/article/pii/S0273117724004423.

[8] Richard Mansergh Thorne. Radiation belt dynamics: The importance of wave-particle interactions. *Geophysical Research Letters*, 37(22), November 2010. ISSN 00948276. doi: 10.1029/2010GL044990. Publisher: Blackwell Publishing Ltd.

[9] M. Sinnhuber, H. Nieder, and N. Wieters. Energetic Particle Precipitation and the Chemistry of the Mesosphere/Lower Thermosphere. *Surveys in Geophysics*, 33(6):1281–1334, November 2012. ISSN 0169-3298, 1573-0956. doi: 10.1007/s10712-012-9201-3. URL http://link.springer.com/10.1007/s10712-012-9201-3.

[10] Frank Toffoletto. Chapter 4 - Modeling techniques. In Vania K. Jordanova, Raluca Ilie, and Margaret W. Chen, editors, *Ring Current Investigations*, pages 99–151. Elsevier, 2020. ISBN 978-0-12-815571-4. doi: https://doi.org/10.1016/B978-0-12-815571-4.00004-4. URL https://www.sciencedirect.com/science/article/pii/B9780128155714000044.

[11] Margaret W. Chen, Colby L. Lemon, James Hecht, Stanislav Sazykin, Richard A. Wolf, Alexander Boyd, and Philip Valek. Diffuse Auroral Electron and Ion Precipitation Effects on RCM-E Comparisons With Satellite Data During the 17 March 2013 Storm. *Journal of Geophysical Research: Space Physics*, 124(6):4194–4216, 2019. ISSN 2169-9402. doi: 10.1029/2019JA026545. URL https://onlinelibrary.wiley.com/doi/abs/10.1029/2019JA026545.

[12] Bernhard Haas, Yuri Y. Shprits, Julia Himmelsbach, Dedong Wang, Alexander Y. Drozdov, Mátyás Szabó-Roberts, and Miroslav Hanzelka. Modeling Pitch Angle Dependent Electron Precipitation Using Electron Lifetimes. *Journal of Geophysical Research: Space Physics*, 129(10):e2024JA032554, 2024. ISSN 2169-9402. doi: 10.1029/2024JA032554. URL https://onlinelibrary.wiley.com/doi/abs/10.1029/2024JA032554.

[13] Yiqun Yu, Shengjun Su, Jinbin Cao, Vania K. Jordanova, and Michael H. Denton. Improved Boundary Conditions for Coupled Geospace Models: An Application in Modeling Spacecraft Surface Charging Environment. *Space Weather*, 20(9):e2022SW003178, 2022. ISSN 1542-7390. doi: 10.1029/2022SW003178. URL https://onlinelibrary.wiley.com/doi/abs/10.1029/2022SW003178.

[14] Bernhard Haas, Yuri Y. Shprits, Hayley J. Allison, Michael Wutzig, and Dedong Wang. A missing dusk-side loss process in the terrestrial electron ring current. *Scientific Reports*, 13(1):970, January 2023. ISSN 2045-2322. doi: 10.1038/s41598-023-28093-2. URL https://www.nature.com/articles/s41598-023-28093-2. Number: 1 Publisher: Nature Publishing Group.

[15] Katja Stoll, Leonie Pick, Dedong Wang, Bernhard Haas, Xing Cao, Binbin Ni, and Yuri Shprits. Can ECH Wave Scattering Explain the Unaccounted Electron Loss During the 17 March 2013 Geomagnetic Storm? *Journal of Geophysical Research: Space Physics*, 130(5):e2024JA033516, 2025. ISSN 2169-9402. doi: 10.1029/2024JA033516. URL https://onlinelibrary.wiley.com/doi/abs/10.1029/2024JA033516.

[16] Katja Stoll, Yangyang Shen, Bernhard Haas, Leonie Pick, Dedong Wang, and Yuri Shprits. The Contribution of Time Domain Structures to Electron Loss During the 17 March 2013 Geomagnetic Storm. *Journal of Geophysical Research: Space Physics*, 131(4):e2025JA034872, 2026. ISSN 2169-9402. doi: 10.1029/2025JA034872. URL https://onlinelibrary.wiley.com/doi/abs/10.1029/2025JA034872.

[17] A. M. Lenchek and S. F. Singer. Geomagnetically trapped protons from cosmic-ray albedo neutrons. *Journal of Geophysical Research (1896-1977)*, 67(4):1263–1287, 1962. ISSN 2156-2202. doi: 10.1029/JZ067i004p01263. URL https://onlinelibrary.wiley.com/doi/abs/10.1029/JZ067i004p01263.

[18] J.-F. Ripoll, S. A. Thaller, D. P. Hartley, D. M. Malaspina, W. S. Kurth, G. S. Cunningham, V. Pierrard, and J. Wygant. Statistics and Models of the Electron Plasma Density From the Van Allen Probes. *Journal of Geophysical Research: Space Physics*, 129(8):e2024JA032528, 2024. ISSN 2169-9402. doi: 10.1029/2024JA032528. URL https://onlinelibrary.wiley.com/doi/abs/10.1029/2024JA032528.

[19] R. B. Horne, T. A. Daggitt, N. P. Meredith, S. A. Glauert, X. Liu, and L. Chen. Measuring Low Plasma Density in the Earth's Equatorial Magnetosphere From Magnetosonic Waves. *Geophysical Research Letters*, 51(12):e2024GL108407, 2024. ISSN 1944-8007. doi: 10.1029/2024GL108407. URL https://onlinelibrary.wiley.com/doi/abs/10.1029/2024GL108407.

[20] Hayley J. Allison, Yuri Y. Shprits, Irina S. Zhelavskaya, Dedong Wang, and Artem G. Smirnov. Gyroresonant wave-particle interactions with chorus waves during extreme depletions of plasma density in the Van Allen radiation belts. *Science Advances*, 7(5):eabc0380, January 2021. doi: 10.1126/sciadv.abc0380. URL https://www.science.org/doi/10.1126/sciadv.abc0380. Publisher: American Association for the Advancement of Science.

[21] Y. Y. Shprits, W. Li, and R. M. Thorne. Controlling effect of the pitch angle scattering rates near the edge of the loss cone on electron lifetimes. *Journal of Geophysical Research: Space Physics*, 111(A12): 12206, December 2006. ISSN 2156-2202. doi: 10.1029/2006JA011758. URL https://onlinelibrary.wiley.com/doi/full/10.1029/2006JA011758. Publisher: John Wiley & Sons, Ltd.

[22] C. F. Kennel and F. Engelmann. Velocity Space Diffusion from Weak Plasma Turbulence in a Magnetic Field. *The Physics of Fluids*, 9(12):2377–2388, December 1966. ISSN 0031-9171. doi: 10.1063/1.1761629. URL https://doi.org/10.1063/1.1761629.

[23] R. B. Horne, S. A. Glauert, and R. M. Thorne. Resonant diffusion of radiation belt electrons by whistler-mode chorus. *Geophysical Research Letters*, 30(9), 2003. ISSN 1944-8007. doi: 10.1029/2003GL016963. URL https://onlinelibrary.wiley.com/doi/abs/10.1029/2003GL016963.

[24] A. Sicard-Piet, D. Boscher, R. B. Horne, N. P. Meredith, and V. Maget. Effect of plasma density on diffusion rates due to wave particle interactions with chorus and plasmaspheric hiss: extreme event analysis. *Annales Geophysicae*, 32(8):1059–1071, August 2014. ISSN 0992-7689. doi: 10.5194/angeo-32-1059-2014. URL https://angeo.copernicus.org/articles/32/1059/2014/.

[25] T. A. Daggitt, R. B. Horne, S. A. Glauert, and G. Del Zanna. Reproducing Ultra-Relativistic Electron Acceleration Using a Coupled Density and Radiation Belt Model. *Journal of Geophysical Research: Space Physics*, 129(12):e2024JA032971, December 2024. ISSN 2169-9402. doi: 10.1029/2024JA032971. URL https://agupubs.onlinelibrary.wiley.com/doi/10.1029/2024JA032971.

[26] Yuri Y. Shprits, Bernhard Haas, and Dedong Wang. Low-density plasma as a key catalyst for electron acceleration in the Van Allen radiation belts. *Communications Physics*, 8(1):314, July 2025. ISSN 2399-3650. doi: 10.1038/s42005-025-02223-w. URL https://www.nature.com/articles/s42005-025-02223-w.

[27] D. A. Subbotin and Y. Y. Shprits. Three-dimensional radiation belt simulations in terms of adiabatic invariants using a single numerical grid. *Journal of Geophysical Research: Space Physics*, 117(5), 2012. ISSN 21699402. doi: 10.1029/2011JA017467. Publisher: Blackwell Publishing Ltd.

[28] H. Volland. A semiempirical model of large-scale magnetospheric electric fields. *Journal of Geophysical Research*, 78(1):171–180, January 1973. ISSN 2156-2202. doi: 10.1029/JA078I001P00171. URL https://onlinelibrary.wiley.com/doi/full/10.1029/JA078i001p00171. Publisher: John Wiley & Sons, Ltd.

[29] David P. Stern. The motion of a proton in the equatorial magnetosphere. *Journal of Geophysical Research*, 80(4):595–599, February 1975. ISSN 2156-2202. doi: 10.1029/JA080I004P00595. URL https://onlinelibrary.wiley.com/doi/full/10.1029/JA080i004p00595.

[30] N. C. Maynard and A. J. Chen. Isolated cold plasma regions: Observations and their relation to possible production mechanisms. *Journal of Geophysical Research*, 80(7):1009–1013, March 1975. ISSN 2156-2202. doi: 10.1029/JA080I007P01009. URL https://onlinelibrary.wiley.com/doi/full/10.1029/JA080i007p01009. Publisher: John Wiley & Sons, Ltd.

[31] N. A. Tsyganenko. A magnetospheric magnetic field model with a warped tail current sheet. *Planetary and Space Science*, 37(1):5–20, 1989. ISSN 00320633. doi: 10.1016/0032-0633(89)90066-4.

[32] B. W. Sheeley, M. B. Moldwin, H. K. Rassoul, and R. R. Anderson. An empirical plasmasphere and trough density model: CRRES observations. *Journal of Geophysical Research: Space Physics*, 106(A11):25631–25641, November 2001. ISSN 2156-2202. doi: 10.1029/2000JA000286. URL https://onlinelibrary.wiley.com/doi/full/10.1029/2000JA000286. Publisher: John Wiley & Sons, Ltd.

[33] Bernhard Haas, Yuri Y. Shprits, Hayley J. Allison, Michael Wutzig, and Dedong Wang. Which Parameter Controls Ring Current Electron Dynamics. *Frontiers in Astronomy and Space Sciences*, 9, 2022. ISSN 2296-987X. URL https://www.frontiersin.org/articles/10.3389/fspas.2022.911002.

[34] Dedong Wang, Yuri Y. Shprits, Irina S. Zhelavskaya, Oleksiy V. Agapitov, Alexander Y. Drozdov, and Nikita A. Aseev. Analytical Chorus Wave Model Derived from Van Allen Probe Observations. *Journal of Geophysical Research: Space Physics*, 124(2):1063–1084, February 2019. ISSN 21699402. doi: 10.1029/2018JA026183. Publisher: Blackwell Publishing Ltd.

[35] Intergovernmental Panel On Climate Change (Ipcc). *Climate Change 2021 – The Physical Science Basis: Working Group I Contribution to the Sixth Assessment Report of the Intergovernmental Panel on Climate Change*. Cambridge University Press, 1 edition, July 2023. ISBN 978-1-009-15789-6. doi: 10.1017/9781009157896. URL https://www.cambridge.org/core/product/identifier/9781009157896/type/book.

[36] Margaret W. Chen, Colby L. Lemon, Timothy B. Guild, Amy M. Keesee, Anthony Lui, Jerry Goldstein, Juan V. Rodriguez, and Phillip C. Anderson. Effects of modeled ionospheric conductance and electron loss on self-consistent ring current simulations during the 5–7 April 2010 storm. *Journal of Geophysical Research: Space Physics*, 120(7):5355–5376, 2015. ISSN 2169-9402. doi: 10.1002/2015JA021285. URL https://onlinelibrary.wiley.com/doi/abs/10.1002/2015JA021285.

[37] G. V. Khazanov, R. M. Robinson, E. Zesta, D. G. Sibeck, M. Chu, and G. A. Grubbs. Impact of Precipitating Electrons and Magnetosphere-Ionosphere Coupling Processes on Ionospheric Conductance. *Space Weather*, 16(7):829–837, 2018. ISSN 1542-7390. doi: 10.1029/2018SW001837. URL https://onlinelibrary.wiley.com/doi/abs/10.1029/2018SW001837.

[38] T. I. Pulkkinen, P. Dredger, M. Liemohn, A. Ridley, G. Tóth, D. Welling, Q. Al Shidi, A. Brenner, S. Hill, and A. Mukhopadhyay. Global MHD Simulations: Magnetosphere–Ionosphere Coupling Dependence on Conductance Model. *Journal of Geophysical Research: Space Physics*, 131(1):e2025JA034675, 2026. ISSN 2169-9402. doi: 10.1029/2025JA034675. URL https://onlinelibrary.wiley.com/doi/abs/10.1029/2025JA034675.

[39] Binbin Ni, Richard M. Thorne, Yuri Y. Shprits, and Jacob Bortnik. Resonant scattering of plasma sheet electrons by whistler-mode chorus: Contribution to diffuse auroral precipitation. *Geophysical Research Letters*, 35(11), 2008. ISSN 1944-8007. doi: 10.1029/2008GL034032. URL https://onlinelibrary.wiley.com/doi/abs/10.1029/2008GL034032.

[40] Dedong Wang, Yuri Y. Shprits, Irina S. Zhelavskaya, Frederic Effenberger, Angelica M. Castillo, Alexander Y. Drozdov, Nikita A. Aseev, and Sebastian Cervantes. The Effect of Plasma Boundaries on the Dynamic Evolution of Relativistic Radiation Belt Electrons. *Journal of Geophysical Research: Space Physics*, 125(5), 2020. ISSN 21699402. doi: 10.1029/2019JA027422.

[41] I. S. Zhelavskaya, N. A. Aseev, and Y. Y. Shprits. A Combined Neural Network- and Physics-Based Approach for Modeling Plasmasphere Dynamics. *Journal of Geophysical Research: Space Physics*, 126 (3), 2021. ISSN 21699402. doi: 10.1029/2020JA028077.

[42] R. E. Denton, Y. Wang, P. A. Webb, P. M. Tengdin, J. Goldstein, J. A. Redfern, and B. W. Reinisch. Magnetospheric electron density long-term (>1 day) refilling rates inferred from passive radio emissions measured by IMAGE RPI during geomagnetically quiet times. *Journal of Geophysical Research: Space Physics*, 117(3), 2012. ISSN 21699402. doi: 10.1029/2011JA017274.

[43] J.-H. Shue, P. Song, C. T. Russell, J. T. Steinberg, J. K. Chao, G. Zastenker, O. L. Vaisberg, S. Kokubun, H. J. Singer, T. R. Detman, and H. Kawano. Magnetopause location under extreme solar wind conditions. *Journal of Geophysical Research: Space Physics*, 103(A8):17691–17700, August 1998. ISSN 2156-2202. doi: 10.1029/98JA01103. URL https://onlinelibrary.wiley.com/doi/full/10.1029/98JA01103.

[44] S. Dubyagin, N. Yu. Ganushkina, I. Sillanpää, and A. Runov. Solar wind-driven variations of electron plasma sheet densities and temperatures beyond geostationary orbit during storm times. *Journal of Geophysical Research: Space Physics*, 121(9):8343–8360, 2016. ISSN 2169-9402. doi: 10.1002/2016JA022947. URL https://onlinelibrary.wiley.com/doi/abs/10.1002/2016JA022947.

[45] W. S. Kurth, S. De Pascuale, J. B. Faden, C. A. Kletzing, G. B. Hospodarsky, S. Thaller, and J. R. Wygant. Electron densities inferred from plasma wave spectra obtained by the Waves instrument on Van Allen Probes. *Journal of Geophysical Research: Space Physics*, 120(2):904–914, 2015. ISSN 2169-9402. doi: 10.1002/2014JA020857. URL https://onlinelibrary.wiley.com/doi/abs/10.1002/2014JA020857.

[46] N. Ganushkina, M. Liemohn, and T. Pulkkinen. Storm-time ring current: model-dependent results. *Journal of Geophysical Research: Space Physics*, 2012. doi: 10.5194/ANGEO-30-177-2012.

[47] M.-C. Fok, N. Y. Buzulukova, S.-H. Chen, A. Glocer, T. Nagai, P. Valek, and J. D. Perez. The Comprehensive Inner Magnetosphere-Ionosphere Model. *Journal of Geophysical Research: Space Physics*, 119(9):7522–7540, 2014. ISSN 2169-9402. doi: 10.1002/2014JA020239. URL https://onlinelibrary.wiley.com/doi/abs/10.1002/2014JA020239.

[48] A. Sciola, V. G. Merkin, K. Sorathia, M. Gkioulidou, S. Bao, F. Toffoletto, K. Pham, D. Lin, A. Michael, M. Wiltberger, and A. Ukhorskiy. The Contribution of Plasma Sheet Bubbles to Stormtime Ring Current Buildup and Evolution of Its Energy Composition. *Journal of Geophysical Research: Space Physics*, 128(11):e2023JA031693, 2023. ISSN 2169-9402. doi: 10.1029/2023JA031693. URL https://onlinelibrary.wiley.com/doi/abs/10.1029/2023JA031693.

[49] YiQun Yu, LongXing Ma, ZiMing Wei, DePeng An, HaiJun Wu, HaoYu Lu, and JinBin Cao. A storm-time ring current model (STRIM). *Science China Technological Sciences*, 67(12):3890–3908, December 2024. ISSN 1869-1900. doi: 10.1007/s11431-024-2654-5. URL https://doi.org/10.1007/s11431-024-2654-5.

[50] Michael Schulz and Louis J. Lanzerotti. Pitch-Angle Diffusion. In *Particle Diffusion in the Radiation Belts*, pages 46–80. Springer Berlin Heidelberg, Berlin, Heidelberg, 1974. ISBN 978-3-642-65675-0. doi: 10.1007/978-3-642-65675-0. URL https://doi.org/10.1007/978-3-642-65675-0.

[51] Yuri Y. Shprits, Adam C. Kellerman, Alexander Y. Drozdov, Harlan E. Spence, Geoffrey D. Reeves, and Daniel N. Baker. Combined convective and diffusive simulations: VERB-4D comparison with 17 March 2013 Van Allen Probes observations. *Geophysical Research Letters*, 42(22):9600–9608, November 2015. ISSN 19448007. doi: 10.1002/2015GL065230. Publisher: Blackwell Publishing Ltd.

[52] J. Himmelsbach, Y. Y. Shprits, H. Allison, B. Haas, M. Wutzig, M. Szabo-Roberts, D. Wang, and A. Y. Drozdov. Using VERB-4D to Model Ring Current Ions and Their Sensitivity to Plasmasphere Density. *Journal of Geophysical Research: Space Physics*, 130(3):e2024JA033128, 2025. ISSN 2169-9402. doi: 10.1029/2024JA033128. URL https://onlinelibrary.wiley.com/doi/abs/10.1029/2024JA033128.

[53] B P Leonard. The ULTIMATE conservative difference scheme applied to unsteady one-dimensional advection. Technical report, 1991. Publication Title: Computer Methods in Applied Mechanics and Engineering Volume: 88.

[54] B P Leonard and H S Niknafs~. SHARP MONOTONIC RESOLUTION OF DISCONTINUITIES WITHOUT CLIPPING OF NARROW EXTREMA. Technical report, 1991. Publication Title: Computers & Fluids Volume: 19 Issue: 1.

[55] Peng Peng, Xin Tao, Zong Peng, Yan Jiang, Zhiming Gao, Di Yang, Jay M. Albert, and Anthony A. Chan. Modeling Radiation Belt Dynamics Using a Positivity-Preserving Finite Volume Method on General Meshes. *Journal of Geophysical Research: Space Physics*, 129(9):e2024JA032919, 2024. ISSN 2169-9402. doi: 10.1029/2024JA032919. URL https://onlinelibrary.wiley.com/doi/abs/10.1029/2024JA032919.

[56] J. M. Albert. Comment on "on the numerical simulation of particle dynamics in the radiation belt. Part I: Implicit and semi-implicit schemes" and "on the numerical simulation of particle dynamics in the radiation belt. Part II: Procedure based on the diagonalization of the diffusion tensor" by E. Camporeale et al. *Journal of Geophysical Research: Space Physics*, 118(12):7762–7764, 2013. ISSN 21699402. doi: 10.1002/2013JA019126.

[57] Alina S. Grishina, Yuri Y. Shprits, Alexander Y. Drozdov, Miriam Sinnhuber, Florian Haenel, Dedong Wang, Mátyás Szabó-Roberts, Jan Maik Wissing, and Stefan Bender. Ring current electron precipitation during the 17 March 2013 geomagnetic storm: Underlying mechanisms and their effect on the atmosphere. *Advances in Space Research*, 73(10):5064–5087, May 2024. ISSN 0273-1177. doi: 10.1016/j.asr.2024.03.010. URL https://www.sciencedirect.com/science/article/pii/S027311772400228X.

[58] M. H. Denton, M. F. Thomsen, V. K. Jordanova, M. G. Henderson, J. E. Borovsky, J. S. Denton, D. Pitchford, and D. P. Hartley. An empirical model of electron and ion fluxes derived from observations at geosynchronous orbit. *Space Weather*, 13(4):233–249, April 2015. doi: 10.1002/2015SW001168. Publisher: Blackwell Publishing Ltd.

[59] Charles F. Kennel. Consequences of a magnetospheric plasma. *Reviews of Geophysics*, 7(1-2):379–419, 1969. ISSN 19449208. doi: 10.1029/RG007i001p00379.

[60] D. A. Subbotin and Y. Y. Shprits. Three-dimensional modeling of the radiation belts using the Versatile Electron Radiation Belt (VERB) code. *Space Weather*, 7(10), 2009. ISSN 1542-7390. doi: 10.1029/2008SW000452. URL https://onlinelibrary.wiley.com/doi/abs/10.1029/2008SW000452.

Supplementary Files

This is a list of supplementary files associated with this preprint. Click to download.

- Supplementary.pdf